ORIGINAL PAPER

Investigation on synergetic effect of non-contact ultrasonic casting and mushy state rolling on microstructure and hardness of Al–Si–Al$_2$O$_3$ nanocomposites

Naveen Kumar Kottana[1] · H. M. Vishwanatha[2] · Srijan Sengupta[3] · Kuldeep Saxena[4] · Ajit Behera[5] · Sudipto Ghosh[1]

Abstract

The present work elucidates a novel way of processing Al–Si–Al$_2$O$_3$ bulk nanocomposites. The novel approach includes synergetic effect of non-contact ultrasonication and mushy state rolling for achieving appreciable uniformity in the distribution of nanoparticles in the metal matrix. A systematic study on the distribution of particles, the resultant microstructure, and also the resultant hardness in the nanocomposite has been presented. It is shown that the current methodology has resulted in enhanced distribution of nanoparticles in the metal matrix as compared to the earlier versions in the field. The structure of the nanocomposites has been explained on the basis of cavitation phenomena and particle pushing during solidification. The work also includes simulation using the Fluent platform to estimate the time available before the initiation of solidification to carry out effective deagglomeration and distribution of nanoparticles in the liquid melt using ultrasonic cavitation. Although the non-contact ultrasonic casting has resulted in a nearly uniform deagglomeration of nanoparticle clusters, a small number of agglomerates were present at the grain boundaries. Hence, the as-cast nanocomposites were deformed in the mushy state condition. An attempt has been made to explore the feasibility of enhancing the distribution of nanoparticles in the Al–Si matrix through semisolid state rolling. The synergetic effect has resulted in enhancement of the hardness of the material by 37%.

Keywords Ultrasonic casting · Cavitation · MMNC · Particle pushing · Solidification · Mushy state rolling · Hardness

✉ H. M. Vishwanatha
  vishwanatha.hm@manipal.edu

1 Department of Metallurgical and Materials Engineering, Indian Institute of Technology-Kharagpur, Kharagpur, WB 721302, India

2 Department of Mechanical and Industrial Engineering, Manipal Institute of Technology-Manipal, Manipal Academy of Higher Education, Manipal, Karnataka 576104, India

3 Department of Metallurgical and Materials Engineering, Indian Institute of Technology-Jodhpur, Jodhpur, Rajasthan 342030, India

4 Department of Mechanical Engineering, GLA University, Mathura, UP 281406, India

5 Department of Metallurgical and Materials Engineering, National Institute of Technology, Rourkela, Odisha 769001, India

1 Introduction

The advent of newer materials consisting of tailored properties is in great demand in recent decades [1]. The thirst for high strength-to-weight ratio materials intended for applications in the automobile industry and aerospace industry is unabated [2]. Metal matrix nanocomposites (MMNCs) developed with tailored mechanical properties perform excellently [3]. Aluminium-alloy based composites are always a lucrative option in this regard. The micro- and nano-sized particles of various oxides, carbides, and nitrides viz., CNT, B$_4$C, SiO$_2$, Al$_2$O$_3$, TiB$_2$, TiC, SiC, Si$_3$N$_4$, etc. are dispersed in Al and Al alloys to produce high performance yet low-density materials [4–6]. However, the processing of MMNCs is a greater challenge owing to the inherent large surface area of nanoparticles resulting in agglomeration [7]. There have been various attempts from researchers around the globe in addressing the tedious challenge of processing MMNCs using techniques based on powder metallurgy,

liquid metallurgy, additive manufacturing, hot deformation, friction stir processing, etc. [8–12]. Broadly the techniques can be grouped as solid-state processing and liquid state processing [13, 14]. As compared to solid state processing, liquid metallurgy based techniques are more beneficial for high volume processing capabilities as it is economical. Thus processing techniques for MMNCs should be based on the aspects of liquid metallurgy. Hence techniques like stir casting and ultrasonic-assisted casting are the most widely used processes for processing MMNCs [15, 16]. However, a few drawbacks are also associated with liquid metallurgy based techniques, viz., heterogeneity in a chemical composition having dendritic microstructure and other casting defects. Although stir casting is simpler and economical for bulk processing, the technique suffers from vortex formation leading to the nominal degree of uniformity in the distribution of nanoparticles. Nanoparticles are strongly bonded and require high energy that can circumvent the forces between particles to deagglomerate [17]. In this regard, the attempt from Yang et al. [18] in processing metal matrix composites by considering ultrasonic energy for deagglomeration was better as compared to the stir casting [18, 19]. The ultrasonic-assisted casting consists of an ultrasonic source capable of generating high-intensity waves that can break the clusters of nanoparticles in the melt [20–22]. However, in the absence of ultrasonic energy, the particles tend to re-agglomerate leading to non-uniformity in the distribution of particles in the metal matrix [23–26]. The resultant mechanical properties are better than those processed by other techniques having the same material composition [27–30]. In recent times several research groups have attempted to process MMNC using contact type ultrasonic-assisted casting effectively, yet the challenge of distribution of nanoparticles homogeneously in the metal matrix persists [31–34]. Hence, in the present work, an attempt has been made for processing the Al–Si–Al$_2$O$_3$ nanocomposite by non-contact ultrasonic casting.

In general, the as-cast products lack desired shape, size, finish, and properties and hence do not fall into the category of the final products. Similarly, the as-cast MMNCs and hence the as-cast bulk MMNCs are processed further through several secondary manufacturing processes to make the final product. The generally followed secondary manufacturing process includes several types of joining and deformation processes [35, 36]. The secondary processing of the as-cast MMNCs results in the elimination of any casting defects, desired shape, size, and tailored mechanical properties in the final product. Rolling is the most widely secondary manufacturing process for processing Al alloys. Often Al alloys are rolled to sheets, plates, and foils. The sheet is used extensively in making the outer body of vehicles, in roofing and sidings of buildings, boat hulls, and in other applications in marine industries. The plate is used for aircraft, civil

Table 1 Chemical composition of Al–Si alloy

Element	Fe	Mg	Si	Al
Wt%	0.62	0.3	3.3	Balance

constructions, military vehicles, oil, refinery, etc. In recent times mushy-state metal forming and MMNC forming processes have been explored on a larger scale as an alternative to conventional rolling processes and also opportunities for innovating metal forming technologies [37, 38]. Mushy state processing involves heating the as-cast product to a state of the two-phased region containing the desired amount of solid–liquid fraction of material and subjecting the material to forming technique [39]. The semisolid state rolling is carried out at smaller flow stresses which is an added advantage to the economics of the secondary processing. Such mushy state rolled products are found to possess refined equiaxed grain structures leading to enhanced mechanical properties [40]. Recent work on semisolid (10–30 vol% liquid) rolling of as-cast Al–4.5Cu based MMC has reported the transformation of rosette-shaped grain structures to equiaxed grains resulting in enhancement of wear and mechanical properties [41–43]. Similar works have also observed improvement in the mechanical performance of the MMC and the enhancement is attributed to work hardening of the matrix [44, 45]. However, limited literature is available on the semisolid processing of Al–Si alloy-based composites. Amongst the other alloys, the hypoeutectic Al–Si alloys are widely used in aerospace, domestic, marine, and automotive applications [46]. The hypoeutectic Al–Si alloys offer good castability and a high strength-to-weight ratio which is a vital property of a material to be considered in making composites. Thus an attempt has been made in the present work to study the synergetic effect of non-contact ultrasonic casting followed by mushy state rolling on the distribution of nanoparticles in the metal matrix and the resultant mechanical properties in the Al–3.3Si–Al$_2$O$_3$ nanocomposites.

2 Materials and methodology

In the present investigation, Al–3.3%Si alloy was used as a matrix. The chemical composition of the alloy is given in Table 1. Into the Al–Si matrix, Al$_2$O$_3$ nanoparticles (Sigma Aldrich, Product Number: 718475) were dispersed via a non-contact ultrasonic casting technique. The average particle size of the alumina powder was around 13 nm, as shown in Fig. 1.
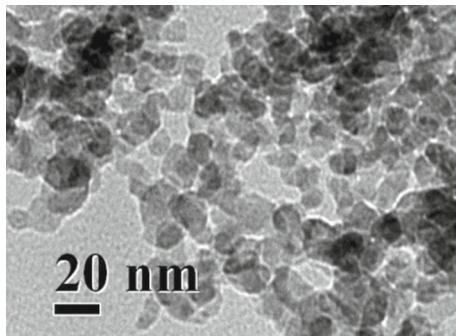
Fig.1 TEM image of Al$_2$O$_3$ nanoparticles

Fig.2 Schematic of Non-contact ultrasonic casting

2.1 Non-contact ultrasonic casting of nanocomposite

The non-contact ultrasonic casting setup used in the current work is different than that used by other research groups [33, 34]. As compared to the earlier setup, the present setup was modified and was designed to achieve a controlled flow of powder and melt, a continuous flow of liquid melt without a drop in the melt temperature till it reaches the mould, dynamic mixing of melt and powder before the content reaches the mould, enhanced reproducibility, and an automated system. The schematic of the experimental setup for synthesizing Al–3.3%Si–1wt% Al$_2$O$_3$ nanocomposite is shown in Fig. 2. The setup consists of a bottom pouring resistance furnace, a runner attached at the bottom of the furnace is placed inside a heating coiled pipe, a vibrator setup connected with a pipe at the bottom, an ultrasonic bath, and a steel mould. The runner connects the vertical pipe and the contents inside mix mechanically as they flow together until they fall into the mould. The nanocomposite was cast in the steel mould surrounded by hot water and placed in the ultrasonic chamber (Bandelin, RK100H, 35 kHz) that sonicates at 35 kHz during processing. The vibrator upon activation will vibrate the sieve that contains the reinforcement mixture. The above-designed setup ensures controlled feed of the reinforcement powder due to motor controlled sieving system, continuous flow of the liquid melt without any appreciable loss of the melt temperature due to the heating coil surrounding the runner, the dynamic mixing of powder in the melt resulting in macro-scale dispersion of nanoparticle agglomerates, enhanced reproducibility and decreased manpower. Initially, the time required for melt to fill the mould and powder particles to fall in to mould were optimized and matched for achieving better dynamic mixing of the contents. The flow rates of melt and the powder were finalized after several iterations of the flow of the contents. For achieving better dispersion in the liquid melt, a carrier powder-based feeding of nanoparticles was introduced. Al powder was used as a carrier powder. The two powders were mixed using
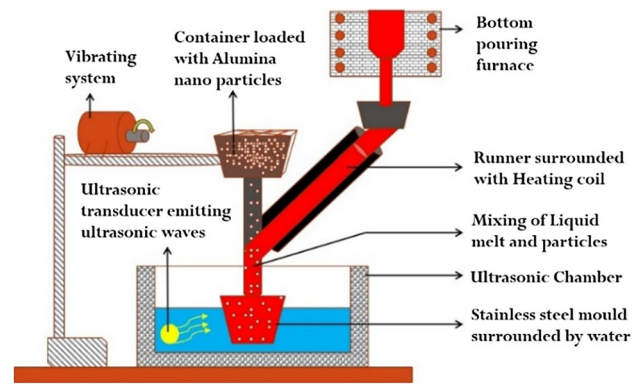
mechanical methods of mixing and as a result, the nanoparticles will get attached with very weak Van der Waals forces to the surface of the carrier powder particle. Such carrier powder-based feeding of nanoparticles results in enhanced micro range dispersion in the melt. During the processing of nanocomposites, initially, pieces of Al-3.3%Si alloy weighing 500 gm were charged in the graphite crucible and placed in the furnace. The temperature of the furnace was raised to 900 °C. While the contents in the furnace were melting, the carrier powder was heated in an oven at 200 °C. Upon completion of the melting of the contents, the top slag layer is removed manually and the preheated powder was loaded into the sieve placed on the vibrator. The bottom pouring was initiated and simultaneously the sieve vibrator and also the ultrasonic bath was activated. As the melt flows through the runner it meets the vertical pipe through the powder particles fall and flow. The powder and the melt mix dynamically in the vertical pipe and the mixture eventually fall into the mould placed at the end of the pipe. The mixture sonicated by the ultrasonic waves is cast. This type of composite casting is referred to as non-contact type ultrasonic casting.

2.2 Mushy state rolling of nanocomposite

A two-high rolling mill with rolls of 120 mm diameter and 125 mm barrel width was used for the mushy state rolling of the composite samples having dimensions of 90 mm × 50 mm × 40 mm. A portable furnace was used to heat the composite samples and feed them into the roller. The schematic of the setup used for mushy state rolling is shown in Fig. 3. The portable furnace has a push rod, the end of which has a pan for holding the composite sample. The furnace has a thermocouple touching the sample surface directly that results in precise temperature control. Selection of rolling temperature plays a vital role in the successful rolling of the samples as excessive heating will lead to higher temperatures of the liquid phase which is undesirable and on the other hand lesser heat will not lead to the formation of a mushy state
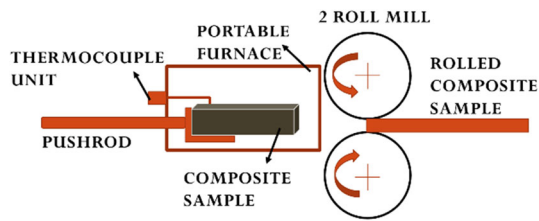
Fig.3 Schematic of portable furnace setup for mushy state rolling of nanocomposite

of the sample. The required temperature was selected based on the Al–Si phase diagram. The selected temperature was 590–600 °C, a temperature corresponding to a 20% liquid fraction. The composite samples were placed on the heating pan of the portable furnace and once the required temperature was achieved, the samples were pushed in between the rolls without any appreciable drop in the temperature. Final rolling was done to 30% reduction in thickness in successive passes and the samples were quenched in water at the end of rolling.

2.3 Characterization and testing of samples

The as-cast Al–Si alloy, Al–Si–Al$_2$O$_3$ nanocomposites, and mushy state rolled nanocomposites were characterized for microstructure and mechanical properties. The samples were ground, polished, and etched using standard metallographic techniques. The microstructure of the etched samples was analyzed under an Optical microscope and FESEM (Zeiss Supra 40; Carl Zeiss) that had a provision for Elemental analysis (EDS, Oxford Instruments). The phases present in the samples were identified by XRD (Panalytical XPert3). The surface of the sample was cleaned and XRD was carried out at a scan speed of 2°/min, at a step size of 0.02. The XRD pattern was analyzed using Xpert-High score software. The hardness of the small samples from different parts of the sample was tested on the Vickers Microhardness tester (UHLVMHT hardness tester). A load of 100 gf was applied on the samples and a dwell time of 15 s was provided during the test. The measured hardness at different points was averaged.

3 Results and discussion

3.1 Phases identification

The XRD analysis was also carried out on both alloy and nanocomposite. The XRD graphs are shown in Fig. 4. The XRD of the Al–Si–Al$_2$O$_3$ composite shows peaks matching the Al$_2$O$_3$ phase confirming the presence of Al$_2$O$_3$ nanoparticles in the Al–Si matrix.
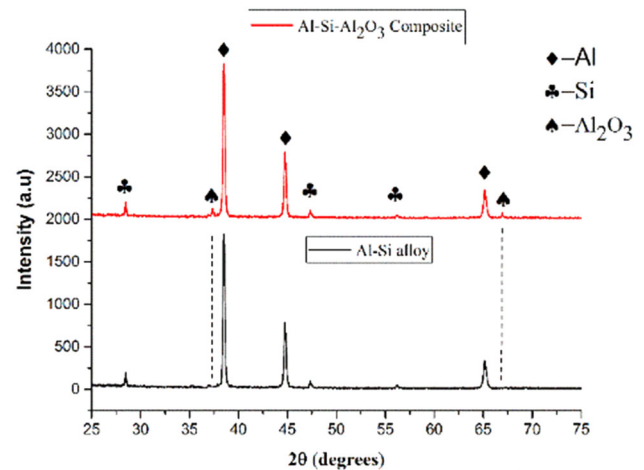

Fig.4 XRD plots of Al–Si alloy and Al–Si–Al$_2$O$_3$ nanocomposite

3.2 Microstructure

The microstructure of the as-cast Al–Si alloy, Al–Si–Al$_2$O$_3$ nanocomposites, and mushy state rolled nanocomposite samples as observed under the optical microscope is shown in Fig. 5. The microstructure of the as-cast alloy taken at $200 \times$ magnification is shown in Fig. 5a. The structure consists of primary aluminum having a dendritic structure with large-sized grains. The large-sized grains having dendritic microstructure are expected to melt initially during heating the material above liquids temperature. Figure 5b shows the microstructure of Al–Si–Al$_2$O$_3$ nanocomposite taken at the same magnification. It is observed that grain refinement has occurred but the dendritic structure persists in the as-cast nanocomposite. Although the nanocomposites were synthesized at similar cooling rates as that of Al–Si alloy, the average grain size in the nanocomposite is less. The grain refinement has occurred by the addition of Al$_2$O$_3$ nanoparticles. The presence of nanoparticles resulted in an increased number of nucleation sites. The nanoparticles act as pinning agents restricting the grain growth resulting in small-sized grains. In addition, non-contact ultrasonication is present at the beginning of the solidification. The ultrasonic waves reaching the liquid melt result in defragmentation of the dendrites that decrease the grain size. The grain refinement has a considerable effect on the hardness of the nanocomposite. Figure 5c shows the microstructure of mushy state rolled Al–Si–Al$_2$O$_3$ nanocomposite. An equiaxed grain structure containing small and big-sized grains can be seen when the composites were heated to mushy state temperature and then rolled. The resultant microstructure in the mushy state rolled nanocomposite is possibly due to rapid solidification, dynamic recrystallization, and grain growth. At the beginning of the rolling process, the material is in a mushy state
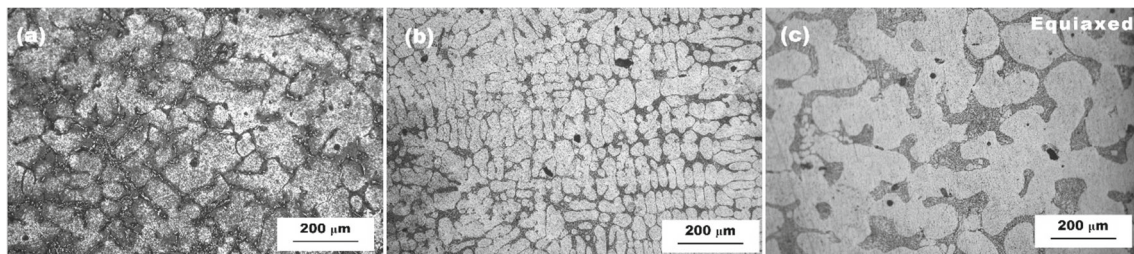
Fig.5 Optical microstructure of **a** as-cast Al–Si alloy, **b** as-cast Al–Si–Al$_2$O$_3$ nanocomposite, and **c** mushy state rolled Al–Si–Al$_2$O$_3$ nanocomposite
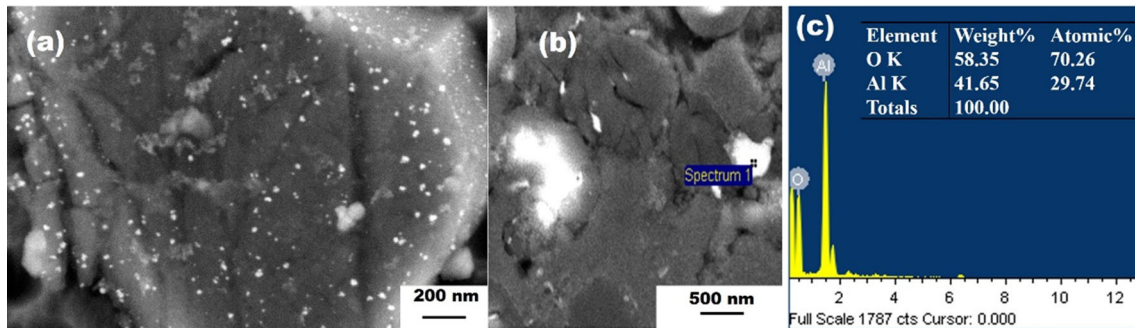

Fig.6 **a** Particle distribution in as-cast Al–Si–Al$_2$O$_3$ nanocomposite, **b** Point chosen for EDX analysis, and **c** EDX analysis

condition consisting of a 20% liquid fraction. As the rolling progresses, the liquid fraction of the material undergoes rapid solidification followed by the nanoparticle-induced dynamic recrystallization which leads to grain fragmentation in the solid fraction. The un-melted solid fraction eventually undergoes coarsening resulting in big-sized grains [41, 47]. In addition, the presence of a 20% liquid fraction allows inter-grain sliding and reorientation.

For a better understanding of the distribution of nanoparticles in the Al–Si matrix, the nanocomposite samples were examined in FE-SEM. Figure 6a shows the microstructure of as-cast Al–Si–Al$_2$O$_3$ nanocomposites synthesized via the non-contact ultrasonic method. The non-contact ultrasonic method has resulted in the appreciable distribution of Al$_2$O$_3$ nanoparticles in the Al–Si matrix. The presence of Al$_2$O$_3$ particles was also confirmed by EDAX analysis. Figure 6b, c shows the EDAX analysis performed. The chosen point for EDX analysis is shown in Fig. 6b and the EDX analysis is shown in Fig. 6c. The EDX analysis confirms that the particle present there is Al$_2$O$_3$. Thus the distribution of Al$_2$O$_3$ particles in the Al–Si matrix is uniform to a greater extent. The uniform distribution is attributed to non-contact ultrasonication resulting in cavitation and non-linear effects [17, 21]. The ultrasonic chamber consists of an ultrasonic sonicator emitting high-energy waves. As the pouring is initiated in the furnace, the ultrasonication is activated. This confirms that the liquid melt experiences ultrasonic energy well before reaching the mould and the ultrasonication is available until the completion of solidification. The high-energy ultrasonic waves reaching the liquid melt result in cavitation and acous-tic streaming phenomenon. The cavitation process results in non-linear effects wherein at a mesoscale, zones of powerful circulations are formed those can result in the exchange of heat at a rapid rate in the convective mode. Such non-linear effects are capable of breaking agglomerates of nanoparticles and dispersing them in the matrix. Hence the uniform distribution of nanoparticles is observed in the nanocomposite.

3.3 Determination of solidification initiation time

To confirm the effect on sonication-induced cavitation in the liquid melt, modeling and simulation of the system were carried out. The simulation is aimed at estimating the solidification start time of liquid melt. The time available before the initiation of the solidification in the mould is predicted. The start time is then compared with the time required for the breaking of nanoparticle clusters. Padhi et al. [33] explained the determination of the time required for breaking nanoparticle agglomerates in the non-contact ultrasonic method.

The determination of solidification initiation time was carried out on the Fluent 6.2 platform. The time was determined based on the liquid fraction contours generated by the simulation. The 2D transient solidification of pure liquid Al–Si was simulated. Figure 7 shows the schematic 2D model of the experimental setup consisting of liquid Al–Si alloy in the steel mold and the boundary conditions.

The top of the liquid metal interface was taken as air and the heat transfer coefficient at this interface was taken as 500 W/m^2 K. No-slip was assumed at the inner wall of the mold. The heat transfer coefficient at the outer wall of the
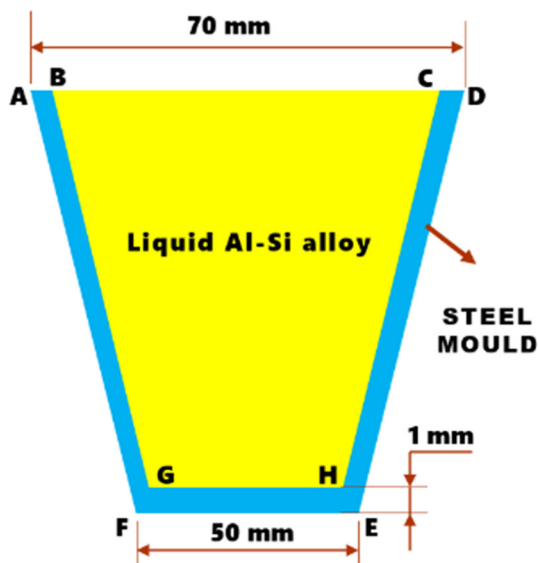
Fig.7 Schematic of mold and liquid metal domain

Table 2 Governing equations and initial/boundary conditions

Item	Equation/data
Governing equations	Continuity equation, Momentum equation, Energy equation (2-Dimensional and in Cartesian coordinate)
Independent variables	x, y, t
Dependent variables	u, v, P, H or T
	Momentum Equation
Computational domain	BCHG (Fig. 7)
Initial condition	$u = 0$, $v = 0$ in the region BCHG (Fig. 7)
Boundary condition	$u = 0$, $v = 0$ along BC, $u = 0$, $v = 0$ along CH, $u = 0$, $v = 0$ along HG, $u = 0$, $v = 0$ along GB
	Energy Equation
Computational domain	ADEF(Fig. 7)
Initial condition	$T = 333$ K in the region ADEF $T = 1173$ K liquid melt region (BCHG)
Boundary condition	$T = T_{ambient}$ along AB, $h = 500$ Wm^{-2} K^{-1} along BC, $h = 8$ Wm^{-2} K^{-1} along CD, $h = 500$ Wm^{-2} K^{-1} along DE, $h = 250$ Wm^{-2} K^{-1} along EF, $h = 500$ Wm^{-2} K^{-1} along FA

mold, surrounded by water, was also taken as 500 W/m^2 K and was considered to be constant throughout the outer surface of the mold. The initial temperature was 333 K throughout the domain excluding molten metal, which was at 1173 K. The governing equations, initial and boundary conditions are given in Table 2. The physical properties of the mould and the liquid Al–Si alloy are given in Tables 3 and 4.

The results of the simulation are shown in Fig. 8. The liquid fractions captured at different time steps are shown in

Table 3 Properties of steel mold

Property	Value(s)
Density (kg/m^3)	8030
Specific Heat (J/kg K)	502.48
Thermal Conductivity (W/m K)	16.27

Table 4 Thermo-physical properties of Al

Property	Parameters	Value(s)
Density(kg/m^3)	Liquid ρ_l at 1173 K	2304
	Solid ρ_s	2699
Specific Heat (J/kg K)	904	
Thermal Conductivity (W/m K)	k_s at 500 K	236
Viscosity (Kg/m s)	1173 K	0.000174
	1073 K	0.000177
	934 K	0.000183
Molecular Weight(kg/mol)	26.98	
Melting Heat (J/kg)	32,100	

Fig. 8a–c. It can be observed that there is no initiation of solidification till the first 10 s after pouring the liquid melt into the mould. At the end of 10 s, a small fraction of solid can be seen at the bottom corners of the mould as observed in Fig. 8b and the appreciable solid fraction is seen at the end of 20 s in Fig. 8c. Thus the time taken for initiation of an appreciable amount of solidification for the given geometry of mould and the given experimental conditions is approximately 20 s. Padhi et al. [33] had estimated the time required for the deagglomeration of clusters of nanoparticles in the liquid melt. The estimated time for initiation of solidification in the current work is 20 s which is much higher than the time required for deagglomeration. By this, it is ensured that deagglomeration occurs much before the initiation of solidification. Thus it is clear that the non-contact ultrasonic casting has resulted in the deagglomeration of the cluster of Al$_2$O$_3$ nanoparticles and in distributing them in the mould.

As the solidification begins and progresses, the solid formed at the walls brings down the intensity of the ultrasonic waves, and hence the deagglomeration and dispersion decrease with the progress in solidification. Although cavitation is present during the pouring and until the initiation of solidification, and the resultant deagglomeration and distribution of nanoparticles has occurred, some amount of grain boundary segregation is observed. The segregation of nanoparticles at grain boundaries is observed due to the liquid-particle pushing effect [31, 32]. At the beginning of the solidification, the liquid is enriched with dispersed nanoparticles. The uniformly dispersed nanoparticles in the liquid melt become the high probability heterogeneous nucleation sites. Random nucleation takes place in all the supercooled regions

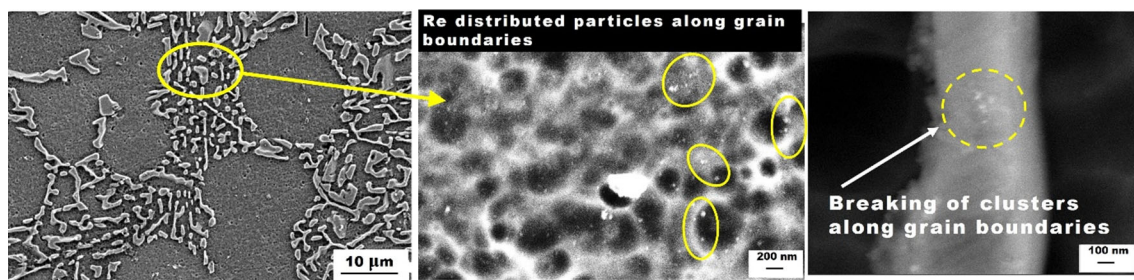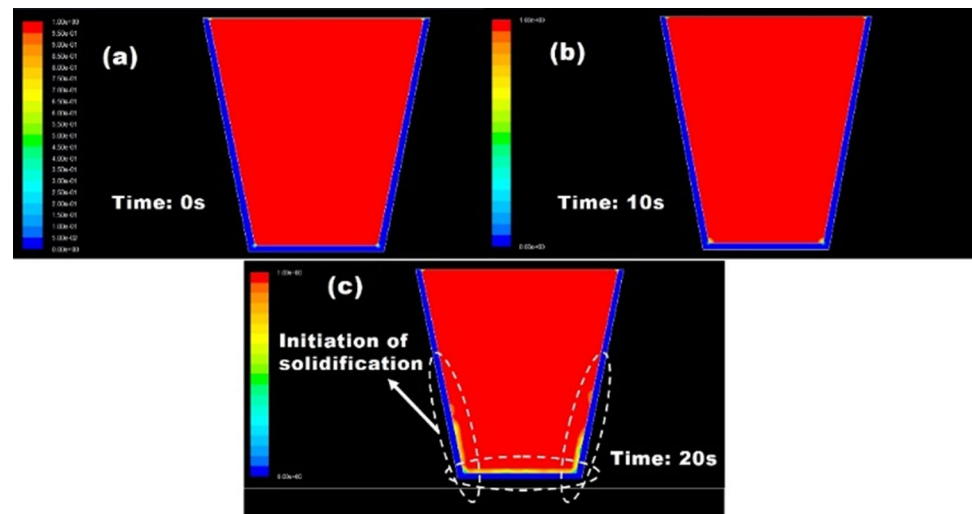**Fig.8** Contours of liquid fraction at **a** t = 0 s, **b** t = 10 s, and **c** t = 10 s

Fig.9 **a** SEM image of Mushy state rolled & quenched Al–Si–Al$_2$O$_3$ nanocomposites taken at lower magnification, **b** Image at higher magnification, and **c** higher magnification image showing breaking of clusters

with the release of latent heat between the new grains. Due to the latent heat released, the cooling rates between the new grains are low and upcoming grains in such decreased cooling rate zones possess a lower solidification front resulting in the pushing effect. Eventually, some amount of grain boundary segregation will be formed. The present work explores the feasibility of mushy state rolling post solidification for the re-distribution of nanoparticles in the nanocomposite formed via non-contact ultrasonic casting.

The effect of mushy state rolling on the distribution of nanoparticles in the Al–Si matrix is shown in Fig. 9a. It appears that the distribution of particles had enhanced further and grain coarsening is also observed. At lower magnification it appears that grain boundary segregation is present. Upon analysis of grain boundary at higher magnifications, shown in Fig. 9(b, c) it is observed that the tiny agglomerates along the grain boundaries are broken and are re-distributed in the Al–Si matrix. Thus it is clear that the mushy state rolling resulted in deagglomeration at grain boundaries segregations. During mushy state rolling, the rapidly solidified sample liquid fraction will be formed at grain boundaries [39, 41, 47]. This liquid melt having nanoparticle agglomerates in it surrounds the un-melted grain boundaries and undergoes plastic deformation when rolled at mushy state temperatures.

This causes the breaking of agglomerates and further particle re-distribution at grain boundaries. From FE-SEM study it is evident that there is a significant amount of uniformity in the dispersion of nanoparticles in Al–Si matrix. The segregated particle agglomerates at the grain boundaries in the nanocomposite were deagglomerated and re-distributed in submicron scale during mushy state rolling. Thus it is clear that mushy state rolling of the nanocomposite can enhance the distribution of the nanoparticles in the matrix resulting in enhanced uniformity in the dispersion of the nanoparticles in the matrix.

3.4 Microhardness

The effect of the addition and distribution of nanoparticles on the hardness property of the material was tested on the Vickers microhardness tester. The microhardness was measured at several locations of the sample and was averaged. The average microhardness of Al–Si alloy, Al–Si–Al$_2$O$_3$ nanocomposite, and mushy state rolled nanocomposite is shown in Fig. 10. It is observed that the addition of nanoparticles has enhanced the hardness of Al–Si alloy. The hardness of the material has increased by 37%. The increase in hardness is attributed to grain refinement induced by the addition
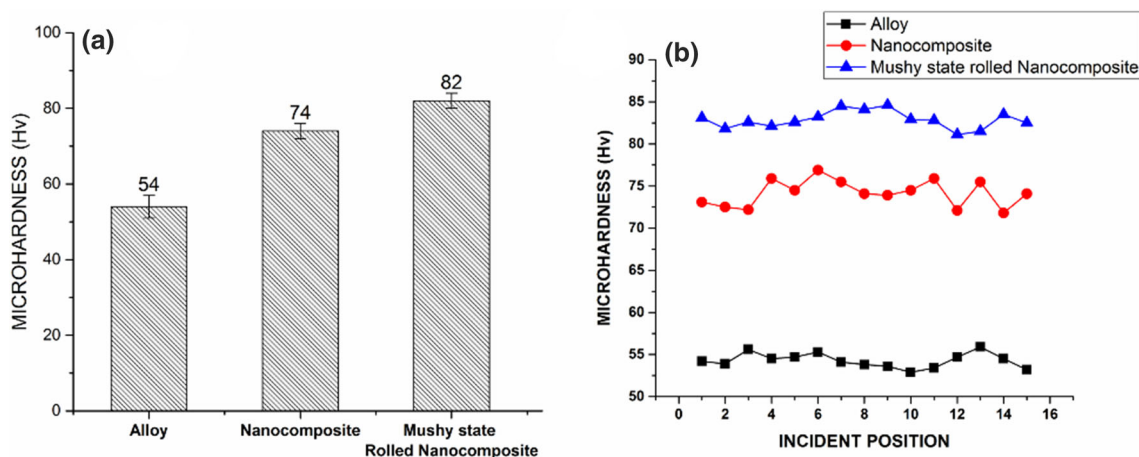
Fig.10 a Variation of microhardness of Al–Si alloy, Al–Si–Al$_2$O$_3$ nanocomposite, and mushy state rolled nanocomposite and **b** distribution of microhardness at different locations of the samples

of nanoparticles. As explained earlier that the addition of nanoparticles via the non-contact ultrasonic method has resulted in a nearly uniform distribution of nanoparticles in the Al–Si matrix. The non-linear effects have resulted in the effective deagglomeration of nanoparticle clusters. The deagglomerated particles become the increased heterogeneous nucleation sites thereby increasing the number of grains and also resulting in grain refinement. Further, the hardness of the nanocomposite has enhanced by 10% upon subjecting to mushy state rolling. Although no extra addition of nanoparticles is carried out to the nanocomposite, an increase in hardness is observed. The additional enhancement in hardness of nanocomposite upon rolling is possibly a result of two effects: (a) rolling induced work hardening and (b) re-breaking of nanoparticle segregation and re-distribution of deagglomerated particles during mushy state rolling.

4 Conclusions

The following conclusions are drawn out of the present work,

1. The non-contact ultrasonic casting technique can be successfully applied to synthesize Al–Si–Al$_2$O$_3$ nanocomposites
2. The resultant microstructures depict appreciable amount of deagglomeration of Al$_2$O$_3$ nanoparticle clusters and also nearly uniform distribution in the Al–Si matrix
3. Although the distribution was nearly uniform and the structure contained fine grains, few segregations due to the pushing effect were observed
4. The resultant finer grains have enhanced the hardness of Al–Si alloy by 37%
5. The mushy state rolling of the so-developed nanocomposites has yielded promising results in further breaking

of nanoparticle agglomerates thereby enhancing the uniformity in distribution of nanoparticles in the Al–Si matrix
6. The hardness of the nanocomposite was further enhanced after mushy state rolling which has been attributed to work hardening and enhanced deagglomeration with redistribution of nanoparticles
7. Synergetic effect of non-contact ultrasonic casting and mushy state rolling can result in good distribution of nanoparticles in the bulk metal matrix and enhanced hardness of the nanocomposite

Declarations

References

1. Shinde, D.M., Sahoo, P.: Fabrication of Aluminium Metal Matrix Nanocomposites: An Overview. Springer, Singapore (2021)
2. Srinivas, V., Jayaraj, A., Venkataramana, V.S., et al.: Mechanical, corrosion and cavitation erosion properties of LM 9 grade aluminium-multi-walled carbon nanotubes composites. Aust. J. Mech. Eng. (2020). https://doi.org/10.1080/14484846.2020.1784557
3. Naik, H.R.M., Mamjunath, L.H., Malik, V., et al.: Effect of microstructure, mechanical and wear on Al-CNTs/graphene hybrid MMC'S. Adv. Mater. Process. Technol. (2021). https://doi.org/10.1080/2374068X.2021.192764
4. Sankhla, A.M., Patel, K.M., Makhesana, M.A., et al.: Experimental investigation of tool wear in machining of SiC based Al-MMC. Adv. Mater. Process. Technol. (2021). https://doi.org/10.1080/2374068X.2021.1948710
5. Vijayan, V., Prabhu, K.N.: The effect of Sr modification on thermal diffusivity of Al–8Si alloy. Int. J. Cast Met. Res. 31, 80–86 (2018). https://doi.org/10.1080/13640461.2017.1367115
6. Vijeesh, V., Prabhu, K.N.: Thermal analysis of cerium-treated chill-cast Al–23 Si alloy. J. Mater. Eng. Perform. 27, 5656–5664 (2018). https://doi.org/10.1007/s11665-018-3670-6
7. Khdair, A.I., Fathy, A.: Enhanced strength and ductility of Al–SiC nanocomposites synthesized by accumulative roll bonding. J. Mater. Res. Technol. 9, 478–489 (2020). https://doi.org/10.1016/j.jmrt.2019.10.077
8. Singh, L., Singh, B., Saxena, K.K.: Manufacturing techniques for metal matrix composites (MMC): an overview. Adv. Mater. Process. Technol. 6, 441–457 (2020). https://doi.org/10.1080/2374068X.2020.1729603
9. Sharma, S., Singh, J., Gupta, M.K., et al.: Investigation on mechanical, tribological and microstructural properties of Al–Mg–Si–T6/SiC/muscovite-hybrid metal-matrix composites for high strength applications. J. Mater. Res. Technol. 12, 1564–1581 (2021). https://doi.org/10.1016/j.jmrt.2021.03.095
10. Sahu, A., Behera, A.: Semi-solid processing and tribological characteristics of Al–Cu Alloy. Mater. Today Proc. 2, 1175–1182 (2015). https://doi.org/10.1016/j.matpr.2015.07.029
11. Behera, A., Patel, S., Priyadarshini, M.: Chapter 7: Fiber-reinforced metal matrix nanocomposites. In: Han, B., Sharma, S., Nguyen, T.A., et al. (eds.) Micro and Nano Technologies, pp. 147–156. Elsevier, Amsterdam (2020)
12. Biswal, S.R., Sahoo, S.: Structural and mechanical properties of a novel Al–Al$_2$O$_3$–WS2 hybrid composites. Mater. Lett. 307, 131017 (2022). https://doi.org/10.1016/j.matlet.2021.131017
13. Das, S., Banthia, S., Patra, A., et al.: Novel bilayer ZnNi/NiCoSiC nanocomposite coating with exceptional corrosion and wear properties by pulse electrodeposition. J. Alloys Compd. 738, 394–404 (2018). https://doi.org/10.1016/j.jallcom.2017.12.093
14. Janakiraman, S., Bhat, K.U.: Formation of composite surface during friction surfacing of steel with aluminium. Adv. Tribol. 2012, 1–6 (2012). https://doi.org/10.1155/2012/614278
15. Ercetin, A., Pimenov, D.Y.: Microstructure, mechanical, and corrosion behavior of Al$_2$O$_3$ reinforced Mg2Zn matrix magnesium composites. Materials 14, 4819 (2021)
16. Swamy, P.K., Mylaraiah, S., GowdruChandrashekarappa, M.P., et al.: Corrosion behaviour of high-strength Al 7005 alloy and its composites reinforced with industrial waste-based fly ash and glass fibre: comparison of stir cast and extrusion conditions. Materials 14, 3929 (2021)
17. Chen, L.-Y., Xu, J.-Q., Choi, H., et al.: Processing and properties of magnesium containing a dense uniform dispersion of nanoparticles. Nature 528, 539–543 (2015). https://doi.org/10.1038/nature16445
18. Yang, Y., Lan, J., Li, X.: Study on bulk aluminum matrix nanocomposite fabricated by ultrasonic dispersion of nano-sized SiC particles in molten aluminum alloy. Mater. Sci. Eng. A 380, 378–383 (2004). https://doi.org/10.1016/j.msea.2004.03.073
19. Manikandan, R., Arjunan, T.V., Akhil, A.R.: Studies on micro structural characteristics, mechanical and tribological behaviours of boron carbide and cow dung ash reinforced aluminium (Al 7075) hybrid metal matrix composite. Compos. Part B Eng. (2020). https://doi.org/10.1016/j.compositesb.2019.107668
20. Yoshitake, Y., Yamamoto, K., Sasaguri, N., Era, H.: Grain refinement of Al–2%Cu alloy using vibrating mold. Int. J. Met. 13, 553–560 (2019). https://doi.org/10.1007/s40962-018-0289-1
21. Flannigan, D.J., Kenneth, S.S.: Plasma formation and temperature measurement during single-bubble cavitation. Nature 434, 52–55 (2005). https://doi.org/10.1038/nature03400.1
22. Gupta, R., Daniel, B.S.S.: Impression creep behaviour of ultrasonically processed in-situ Al3Zr–Al alloy composite in as-cast condition. Mater. Charact. 169, 110594 (2020). https://doi.org/10.1016/j.matchar.2020.110594
23. Arunkumar, T., Selvakumaran, T., Subbiah, R., et al.: Development of high-performance aluminium 6061/SiC nanocomposites by ultrasonic aided rheo-squeeze casting method. Ultrason. Sonochem. 76, 105631 (2021). https://doi.org/10.1016/j.ultsonch.2021.105631
24. Chen, M., Liu, Z.: Ultrasound assisted casting method for fabricating B4Cp/Al composites with the addition of K2ZrF6. Mater. Lett. 280, 128545 (2020). https://doi.org/10.1016/j.matlet.2020.128545
25. Chen, M., Liu, Z., Zheng, Q., et al.: Rapid preparation of B4Cp/Al composites with homogeneous interface via ultrasound assisted casting method. J. Alloys Compd. 858, 157659 (2021). https://doi.org/10.1016/j.jallcom.2020.157659
26. Li, Z., Jiang, R., Li, X., et al.: Microstructural evolution and wear behavior of SiCp/7085 composites manufactured by ultrasonic stirring casting. Metals (Basel) (2020). https://doi.org/10.3390/met10050650
27. Malaki, M., Tehrani, A.F., Niroumand, B., Abdullah, A.: Ultrasonically stir cast SiO2/A356 metal matrix nanocomposites. Metals (Basel) (2021). https://doi.org/10.3390/met11122004
28. Pradeep Kumar, J., Robinson Smart, D.S., Stephen Manova., Ummal Salmaan, N.: Effect of TaC/Ti/Si$_3$N$_4$ hard ceramics on mechanical and microstructural behaviour of AA7075 processed through stir casting process. Adv. Mater. Sci. Eng. 2022, 6804011 (2022). https://doi.org/10.1155/2022/680401
29. Rao, T.B.: Microstructural, mechanical, and wear properties characterization and strengthening mechanisms of Al7075/SiCnp composites processed through ultrasonic cavitation assisted stir-casting. Mater Sci Eng A 805, 140553 (2021). https://doi.org/10.1016/j.msea.2020.140553
30. Wang, H., Hu, Y., Ning, F., Cong, W.: Ultrasonic vibration-assisted laser engineered net shaping of Inconel 718 parts: effects of ultrasonic frequency on microstructural and mechanical properties. J. Mater. Process. Technol. 276, 116395 (2020). https://doi.org/10.1016/j.jmatprotec.2019.116395
31. Vishwanatha, H.M., Eravelly, J., Kumar, C.S., Ghosh, S.: Microstructure and mechanical properties of aluminum-alumina bulk nanocomposite produced by a novel two-step ultrasonic casting technique. Metall. Mater. Trans. A 47, 5630–5640 (2016). https://doi.org/10.1007/s11661-016-3740-z
32. Vishwanatha, H.M., Eravelly, J., Kumar, C.S., Ghosh, S.: Dispersion of ceramic nano-particles in the Al–Cu alloy matrix using two-step ultrasonic casting and resultant strengthening. Mater. Sci.

Eng. A **708**, 222–229 (2017). https://doi.org/10.1016/j.msea.2017.09.117

33. Padhi, P., Kumar, K.N., Ghosh, S., et al.: Modeling and experimental validation of deagglomeration of ultrafine nanoparticles in liquid al during noncontact ultrasonic casting of Al–Al$_2$O$_3$ Nanocomposite. Mater. Manuf. Process. **31**, 1589–1596 (2016). https://doi.org/10.1080/10426914.2015.1004707

34. Mula, S., Padhi, P., Panigrahi, S.C., et al.: On structure and mechanical properties of ultrasonically cast Al–2%Al$_2$O$_3$ nanocomposite. Mater. Res. Bull. **44**, 1154–1160 (2009). https://doi.org/10.1016/j.materresbull.2008.09.040

35. Verma, S., Gupta, M., Misra, J.P.: Effect of preheating and water cooling on the performance of friction-stir-welded aviation-grade aluminum alloy joints. J. Mater. Eng. Perform. **28**, 4209–4220 (2019). https://doi.org/10.1007/S11665-019-04183-Z

36. Verma, S., Misra, J.P.: Experimental investigation on friction stir welding of dissimilar aluminium alloys. Proc. Inst. Mech. Eng. Part E J. Process. Mech. Eng. **235**, 1545–1554 (2021). https://doi.org/10.1177/09544089211008694

37. Rovira, M.M., Lancini, B.C., Robert, M.H.: Thixo-forming of Al–Cu alloys. J. Mater. Process. Technol. **92–93**, 42–49 (1999). https://doi.org/10.1016/S0924-0136(99)00220-4

38. Zu, L., Luo, S.: Study on the powder mixing and semi-solid extrusion forming process of SiCp/2024Al composites. J. Mater. Process. Technol. **114**, 189–193 (2001). https://doi.org/10.1016/S0924-0136(01)00738-5

39. Siddhalingeshwar, I.G., Herbert, M.A., Chakraborty, M., Mitra, R.: Effect of mushy state rolling on age-hardening and tensile behavior of Al–4.5Cu alloy and in situ Al–4.5Cu–5TiB2 composite. Mater. Sci. Eng. A **528**, 1787–1798 (2011). https://doi.org/10.1016/j.msea.2010.11.027

40. Atkinson, H.V., Burke, K., Vaneetveld, G.: Recrystallisation in the semi-solid state in 7075 aluminium alloy. Mater. Sci. Eng. A **490**, 266–276 (2008). https://doi.org/10.1016/j.msea.2008.01.057

41. Herbert, M.A., Sarkar, C., Mitra, R., Chakraborty, M.: Microstructural evolution, hardness, and alligatoring in the Mushy state rolled cast Al–4.5Cu alloy and In-situ Al4.5Cu–5TiB$_2$ composite. Metall. Mater. Trans. A Phys. Metall. Mater. Sci. **38**, 2110–2126 (2007). https://doi.org/10.1007/s11661-007-9264-9

42. Herbert, M.A., Maiti, R., Mitra, R., Chakraborty, M.: Wear behaviour of cast and mushy state rolled Al–4.5Cu alloy and in-situ Al4.5Cu–5TiB$_2$ composite. Wear **265**, 1606–1618 (2008). https://doi.org/10.1016/j.wear.2008.03.010

43. Herbert, M.A., Das, G., Maiti, R., et al.: Tensile properties of cast and mushy state rolled Al–4·5Cu alloy and in situ Al4·5Cu–5TiB$_2$ composite. Int. J. Cast Met. Res. **23**, 216–224 (2010). https://doi.org/10.1179/136404609X12580240349018

44. Chawla, K.K., Metzger, M.: Initial dislocation distributions in tungsten fibre-copper composites. J. Mater. Sci. **7**, 34–39 (1972). https://doi.org/10.1007/BF00549547

45. Arsenault, R.J., Shi, N.: Dislocation generation due to differences between the coefficients of thermal expansion. Mater. Sci. Eng. **81**, 175–187 (1986). https://doi.org/10.1016/0025-5416(86)90261-2

46. Ye, H.: An overview of the development of Al–Si-Alloy based material for engine applications. J. Mater. Eng. Perform. **12**, 288–297 (2003). https://doi.org/10.1361/105994903770343132

47. Mandal, M., Mitra, R.: Effect of mushy state rolling on the microstructure, microhardness, and microtexture in Al–4.5wt.%Cu–5wt.%TiB2 in situ composite. Jom **68**, 1902–1908 (2016). https://doi.org/10.1007/s11837-016-1911-4